Hindawi
Shock and Vibration
Volume 2023, Article ID 4340874, 18 pages
https://doi.org/10.1155/2023/4340874

Research Article

Analysis of Fluid-Structure Coupling Vibration Characteristics of Pipeline Transporting Bubbly Fluid Medium: With Application to Luxury Passenger Ship Life Area Pipeline

Chen Chen, Hong Zhou, and Lei Zhang

College of Naval Architecture and Ocean Engineering, Jiangsu University of Science and Technology, Zhenjiang 212100, China

Correspondence should be addressed to Chen Chen; 201010006@stu.just.edu.cn and Hong Zhou; 199600001373@just.edu.cn

Received 8 November 2022; Revised 21 December 2022; Accepted 11 January 2023; Published 30 January 2023

Academic Editor: Furen Ming

When pipelines are transporting bubbly fluid medium, due to the coalescence and breakage behaviours of the bubbles, the pressure distribution at the wall is not uniform and the structure response is more complex. The bubbly beverage pipeline in the life area of the luxury passenger ship is a typical scene of the pipeline transporting bubbly fluid medium. In this paper, the two-way fluid-structure coupling analysis is carried out on such a scene with the aid of ANSYS software and the PBM model is introduced to characterize the dynamic properties of bubbles. At the same time, the accuracy of this calculation method is verified by the scaling experiment. On this basis, the response of the pipeline under the excitation of bubbly fluid is calculated for different inlet velocities and gas volume fractions, and the effectiveness of common vibration damping measures is evaluated. The result shows that the addition of bubbles to the fluid medium has a significant effect on the distribution of the flow field in the pipeline during transport, and the vibration acceleration values of the pipe wall also increase significantly. This method enables accurate simulation of the vibration characteristics of bubbly fluid medium pipelines.

1. Introduction

Fluid transportation pipelines are widely used in many industries, such as petrochemical, aerospace, marine engineering, and agricultural irrigation, which effectively promote the reform and development of these industries [1–3]. For the marine engineering industry, the pipeline system plays the role of connecting various key equipment, which is directly related to the functional integrity of the delivered products. However, in the actual use of equipment, abnormal vibrations often occur due to the interaction between the internal fluid of the pipeline and the external wall [4–6]. Especially for high-value-added passenger ships represented by luxury passenger ships, due to the complexity of their system functions, the layout density of pipelines is much higher than that of conventional marine products, the load situation is more complex, and abnormal vibrations are more likely to occur. Among them, the beer and carbonated beverage pipeline in the life area is a typical scene of transporting bubbly fluid medium. Due to the addition of bubbles, the form of action between the fluid medium and the pipe wall is more complex. It is necessary to investigate the vibration characteristics to provide a reference for the vibration damping design of the pipeline.

For the study of pipeline flow-induced vibration, many scholars have made a lot of exploration combined with their fields. The research on the vibration characteristics of fluid pipelines could be traced back to 1809. Young [7] studied the pressure wave propagation characteristics in the wall structure of elastic liquid-filled pipelines, which inspired subsequent research on the pressure wave theory. Later, Korteweg, Halliwell, and Wylie considered the influence of liquid compressibility, pipe wall elasticity, and end constraints on pipeline vibration characteristics on this basis [8]. In 1898, Joukowsky [9] considered the influence of the pipe wall on fluid pressure waves and derived the classic basic formula of water hammer motion, which is widely used in the industrial field. However, all the studies so far only

consider the excitation of the pipe wall by the fluid and ignore the influence of the pipe deformation on the fluid movement, which leads to large errors in some calculation scenarios. Therefore, in the following studies, relevant scholars determined the interaction modes between the fluid and the pipe wall, mainly including the following four types [10, 11], including Poisson coupling [12, 13], friction coupling [14–16], junction coupling [17–19], and Bourdon coupling [20–22].

Based on determining the basic form of fluid-structure coupling, the relevant scholars abstracted the vibration model of the pipeline into the beam model and the shell model based on the size characteristics (length/diameter, thickness, etc.) of the pipe and established the control equation based on the momentum conservation equation and the continuity equation to solve and derive the vibration solution methods such as the characteristic line method [23], the impedance analysis method, the modal analysis method [24], and the transfer matrix method [25]. However, these methods are usually suitable for solving the vibration characteristics of a single fluid medium in pipelines and are difficult to meet the demands of a multiphase flow solution.

With the rapid development of computing technology, domestic and foreign scholars have done a lot of research on fluid-structure coupling vibration of the pipeline by a numerical calculation method. Among them, the finite element method and finite volume method are more representative. The finite element method could solve the structural response, and the finite volume method could accurately predict the flow field characteristics. Therefore, the combination of the two methods could conveniently analyze the bidirectional fluid-structure coupling vibration of pipelines. In addition, with the aid of continuous development of multiphase flow models, this calculation method could conveniently calculate the flow-induced vibration characteristics of pipeline multiphase flow, which made up for the deficiency of the above analytical calculation method to some extent [26–28].

The key to studying the vibration characteristics of the pipeline transporting bubbly fluid medium is to represent the dynamic properties of the bubbles. However, in the existing multiphase flow analysis of pipelines, the Eulerian-Eulerian heterogeneous flow model and hybrid model [29] are usually used, but it is difficult to consider the bubble coalescence and fracture evolution process in the pipeline. To better simulate this flow pattern, the population balance model (PBM) was introduced in this paper.

The population balance model (PBM) was used to describe the development of groups with similar features. Also, it was widely used in the chemistry field to describe the flow characteristics such as fluidized beds and bubbling towers [30, 31]. In addition, in the field of hydraulic machinery, the PBM model was also applied to the simulation of cavitation in the flow channel of the water pump, which provided a reference for the structure of the water pump [32, 33]. The above examples show that the PBM model can simulate the flow characteristics of the bubbly fluid, and its simulation accuracy can meet the requirements of mechanical structure design optimization.

In this paper, the coalescence and breakage of bubbles were simulated based on the PBM model, and the flow field distribution of high gas-liquid fluid was obtained. On this basis, the force-displacement transfer of fluid and pipe wall was carried out, and the transient vibration response law of pipe wall was studied, which could provide a reference for structural optimization in practical engineering applications.

2. Mathematical Model

In this paper, a two-fluid model and a PBM model were introduced to describe the motion of the fluid in the pipeline. The two-fluid model was used to calculate the turbulent energy dissipation rate, gas content, and flow field, which were used to calculate the bubble aggregation and breakage rates and thus to solve the PBM equation. The PBM equation was used to calculate the size of the bubbles and thus to calculate the interaction forces between the bubbles and to correct the turbulence source term in the two-fluid model due to bubble turbulence. The coupling model is shown in Figure 1.

2.1. Population Balance Model. The high gas pipeline (such as beverage pipelines) in the life area studied in this paper had the phenomenon of bubble coalescence and breakage in the flow process. The PBM model can be used to predict this phenomenon of bubbles and solve the pressure distribution in the flow process. The general form of the PBM can be expressed as follows [34]:

$$\frac{\partial}{\partial t}[n(V,t)] + \nabla \cdot [\vec{u} n(V,t)] + \nabla_v \cdot [G_v n(V,t)] = \frac{1}{2}\int_0^V a\left(V - V', V'\right) n\left(V - V', t\right) n\left(V', t\right) \mathrm{d}V' \quad (1)$$

$$- \int_0^\infty a\left(V, V'\right) n(V,t) n\left(V', t\right) \mathrm{d}V' + \int_{\Omega_v} p g\left(V'\right) \beta\left(V \mid V'\right) n\left(V' t\right) \mathrm{d}V' + g(V) n(V,t),$$

① ② ③ ④

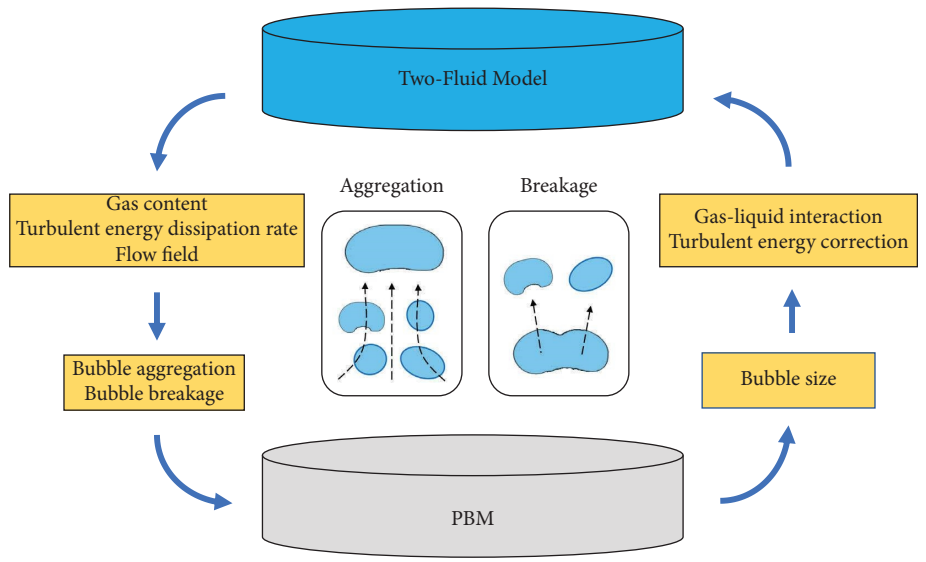

Figure 1: Diagram of the coupling model.

where V' is the initial bubble volume, V is the sub-bubble volume, $a(V, V')$ is the collision frequency between bubbles, $g(V')$ is the breaking frequency, and $\beta(V|V')$ is the probability density of the bubble breaking from volume V' to volume V.

Among them, ① represents the birth of bubbles due to aggregation and ② represents the death of them. ③ and ④ represent the birth and death of bubbles due to breakage, respectively.

2.2. Solution for Population Balance Model. For the population balance equation discussed above, it usually can be solved in four methods, like the discrete method, the inhomogeneous discrete method, the standard method of moments, and the quadrature method of moments. To define the typical diameters of bubbles, this paper used the discrete method to solve the population balance equation, and the main solving steps are as follows.

The population balance equation can be written as equation (2) in terms of volume fraction of bubbles of size i.

$$\frac{\partial}{\partial t}(\rho_s \alpha_i) + \nabla \cdot (\rho_s u_i \alpha_i) + \frac{\partial}{\partial V}\left(\frac{G_v \rho_s \alpha_i}{V}\right) = \rho_s V_i \left(B_{ag,i} - D_{ag,i} + B_{br,i} - D_{br,i}\right) + 0^i \rho_s V_0 \dot{n}_0, \tag{2}$$

where ρ_s is the density of the gas, $\dot{n}_0$ is the nucleation rate for the volume fraction of the smallest bubble size V_0, and α_i is the volume fraction of bubbles of size i, which is defined as

$$\begin{aligned} \alpha_i &= N_i V_i, \quad i = 0, 1, \ldots, N-1, \\ N_i(t) &= \int_{V_i}^{V_{i+1}} n(V, t) \mathrm{d}V, \end{aligned} \tag{3}$$

where V_i is the volume of bubbles of size i.

The growth rate in equation (2) can be discretized as follows [35]:

$$\frac{\partial}{\partial V}\left(\frac{G_v \rho_s \alpha_i}{V}\right) = \rho_s V_i \left[\left(\frac{G_{v,i-1} N_{i-1}}{V_i - V_{i-1}}\right) - \left(\frac{G_{vi} N_i}{V_{i+1} - V_i}\right)\right], \tag{4}$$

where $V_{i+1}/V_i = 2^q$ and the ratio is defined as the "ratio factor."

The birth and death rates of bubbles can be defined as follows:

$$\begin{aligned} B_{ag,i} &= \sum_{k=1}^{N} \sum_{j=1}^{N} a_{kj} N_k N_j x_{kj} \xi_{kj}, \\ D_{ag,i} &= \sum_{j=1}^{N} a_{ij} N_i N_j n, \\ B_{br,i} &= \sum_{j=i+1}^{N} g(V_j) N_j \beta\left(V_i \middle| V_j\right), \\ D_{br,i} &= g(V_i) N_i n, \end{aligned} \tag{5}$$

where $a_{ij} = a(V_i, V_j)$ and

$$\xi_{kj} = \begin{cases} 1, & \text{for } V_i < V_{ag} < V_{i+1}, \text{ where } i \le N-1, \\ 0, & \text{otherwise.} \end{cases} \tag{6}$$

In equation (6), V_{ag} is the bubble volume resulting from the aggregation of bubbles k and j and is defined as

$$V_{ag} = \left[x_{kj}V_i + \left(1 - x_{kj}\right)V_{i+1}\right],$$
$$x_{kj} = \frac{V_{ag} - V_{i+1}}{V_i - V_{i+1}}, \tag{7}$$

2.3. Birth and Death of Bubbles due to Breakage and Aggregation. The birth and death of bubbles occur due to breakage and aggregation, and the process in the pipelines can be characterized by the following equations.

The breakage rate of bubbles can be expressed as [36]

$$\Omega_{br} = F_B g\left(V^{'}\right)\beta\left(V \mid V^{'}\right), \tag{8}$$

where $g(V^{'})$ is the breakage frequency, $\beta(V \mid V^{'})$ is the probability density function of bubbles breaking from volume V to volume $V^{'}$, and F_B is the breakage factor for the calibration of the breakage kernels.

The birth rate of bubbles of volume V can be expressed as

$$D_{br} = g(V)n(V). \tag{9}$$

In the equations above, the probability density function $\beta(V \mid V^{'})$ needs to meet the following constraints.

(1) For the normalization condition,

$$\int_0^{V^{'}} \beta\left(V \mid V^{'}\right)\mathrm{d}V = 1. \tag{10}$$

(2) For conservation of mass,

$$p\int_0^{V^{'}} m(V)\beta\left(V \mid V^{'}\right)\mathrm{d}V = m\left(V^{'}\right). \tag{11}$$

(3) For binary breakage, V and $V^{'}$ are symmetric, and we can get

$$\beta\left(V^{'} - V \mid V^{'}\right) = \beta\left(V \mid V^{'}\right). \tag{12}$$

The above is the breakage process of bubbles. For the aggregation process, the aggregation kernel can be expressed as [36]

$$\Omega_{ag} = F_A a\left(V, V^{'}\right), \tag{13}$$

where F_A is the aggregation factor for the calibration of the aggregation kernels.

The birth rate of bubbles of volume V is given by

$$B_{ag} = \frac{1}{2}\int_0^{V} a\left(V - V^{'}, V^{'}\right)n\left(V - V^{'}\right)n\left(V^{'}\right)\mathrm{d}V^{'}, \tag{14}$$

where bubbles of volume $V - V^{'}$ aggregate with bubbles of volume $V^{'}$ to bubbles of volume V and the coefficient 1/2 in equation (14) is induced to avoid the repeated occurrence of the collision.

The death rate of bubbles of volume V due to aggregation can be expressed as

$$D_{ag} = \int_0^{\infty} a\left(V, V^{'}\right)n(V)n\left(V^{'}\right)\mathrm{d}V^{'}. \tag{15}$$

3. Numerical Simulation Procedures

3.1. Pipeline Model. This paper focused on the analysis of the vibration of the pipeline under internal bubbly fluid slamming. The common pipeline system was composed of straight pipe and pipeline fittings assembled and welded. The pipeline bending and the change of the pipe diameter in the direction of the pipeline were likely to cause the change of the fluid inside, leading to the abnormal vibration of the pipeline system. Especially for the pipeline system in the life area of luxury passenger ships studied in this paper, the pipeline with special functions undertakes the transmission function of the bubbly fluid medium (e.g., beer pipelines in the life area), and the pressure of the internal flow field is more complicated. Under its driving, the vibration form of the external pipe wall is also more diverse. In delivered shipbuilding projects, this type of pipeline suffered from higher vibration than the conventional one. So, it was necessary to study the vibration form of the pipeline system under such operating conditions.

In this paper, a part of the structure of the ship life area was selected as the object of study, as shown in Figure 2. This structure mainly contained straight pipes, bends, reducers, and supports, and the relevant dimensional values are shown in Figure 3. The role of this pipeline was to transport fluid containing bubbles such as beer and cola. The diameter was determined based on the actual volume of fluid transported. The relevant dimensional parameters were derived from the actual ship model. Firstly, the inner diameter of the beginning straight pipeline was 400 mm. Next, the inner diameter of the line was reduced to 180 mm with the transition of a reducer. Finally, two short straight pipes and a 90° elbow were connected to reach the outlet area. The inner diameter of the pipeline was kept constant.

In addition, the relevant calculations were based on an operating condition of 22°C, and the material parameters of the pipe wall and supports are shown in Table 1. To improve the reproduction of the numerical simulation to the actual working conditions, the boundary conditions needed to be set appropriately. Under common support principles, supports were provided at the beginning and end of long spans of straight pipe with fixed end restraints. In addition, the inlet was usually welded to an accessory such as the pump or other pipeline. So, this paper applied fixed restraint at the inlet to simulate the boundary conditions.

3.2. Calculation Method. In this paper, the data transfer relationship between the Fluent module and the Mechanical module was established based on the ANSYS software ecology, and the two-phase implicit iterative method was used for the fluid-structure coupling vibration analysis of the pipeline. Both the structure and the fluid were solved in their

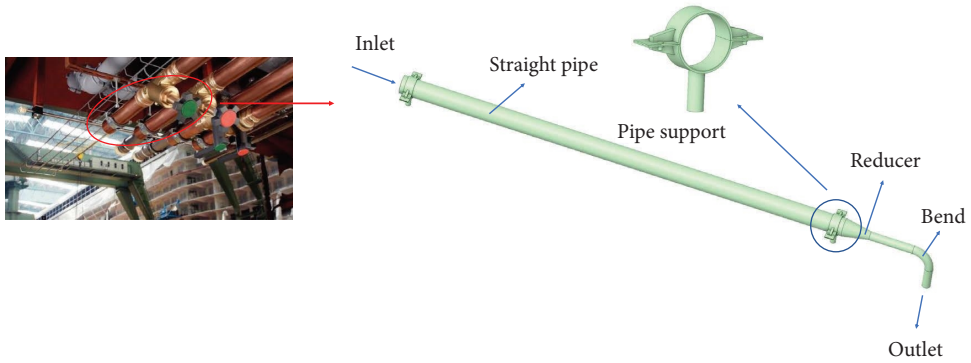

Figure 2: Schematic diagram of pipeline structure form.

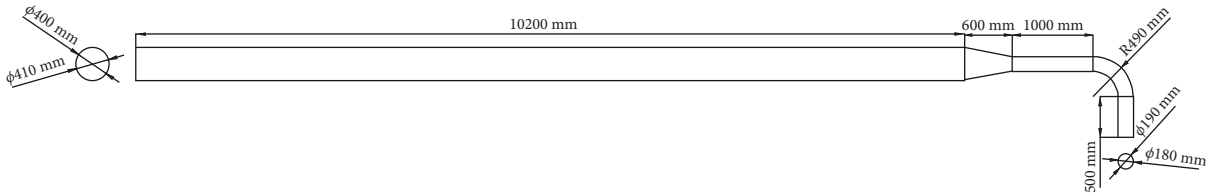

Figure 3: Dimensional diagram of the pipeline structure.

Table 1: Material parameters of the pipeline structure.

Components	Density (kg/m^3)	Poisson's ratio	Young's modulus (MPa)	Yield strength (MPa)
Pipe wall	7750	0.31	$1.93e+5$	207
Supports	7850	0.3	$2e+5$	250

respective modules, with the structure being solved using the finite element method and the flow field being solved using the finite volume method. In each time step, the flow field transmitted the calculated results in the form of loads to the structural field through the fluid-structure interface, and the vibrations generated by the structural field under the influence of the flow field loads were transmitted to the flow field in the form of loads, and so on, repeatedly iterating to reach a certain convergence standard before moving on to the next time step, as shown in Figure 4.

3.3. Grid Generation. The pipeline models described in this paper were all gridded based on the ANSYS mesh module. The fluid domain was dominated by the structured grid, and the expansion was near the pipe wall to improve the accuracy of the calculation in the fluid boundary layer region. The solid domain was also dominated by the structured grid and scaled to match the fluid domain to improve the grid node matching. Based on the determination of the gridding method for both the fluid and solid domains, this paper performed a grid-independent verification to exclude the influence of the number of grids on the accuracy of the calculation.

The pipeline configuration and its material used for grid-independent verification were described in Section 3.2. The fluid medium in the pipeline was water and carbon dioxide. The inlet type was a velocity inlet with a flow rate of 2 m/s for both water and carbon dioxide. The carbon dioxide was in the form of bubbles with a diameter of 1.1 to 1.2 mm and an overall volume fraction of 0.2, and the aggregation and breakage kernel behaviours were described by the Luo model [36]. The outlet type was a pressure outlet with no backflow for the water and carbon dioxide bubbles.

To assess the reasonableness of the gridding, the maximal displacement at a point in the middle of the straight pipe section (as shown in Figure 5) was selected as an observation in this paper to study the effect of different grid quantities on its maximal displacement values.

The grid-independent validation method used in this paper was to study the relationship between the number of grids and the monitoring values selected above on the basis of ensuring the basic structured grid and the expansion layer structure. The number of grids was controlled by grid size adjustment, and the results of grid verification are shown in Figure 6.

Figure 6 shows the relationship between the number of grids and the maximal displacement of the selected monitoring point. In this paper, calculations were carried out for eight cases in the range of mesh cell sizes from 90 mm to 20 mm. As shown in Figure 7, the values of the maximal displacements tend to stabilize when the grid size exceeds 60 mm. When the grid size is further reduced to 20 mm, the calculated maximal displacement values instead show an increase in error. Therefore, to balance the efficiency and accuracy of the calculations, the grid size was 60 mm. At this

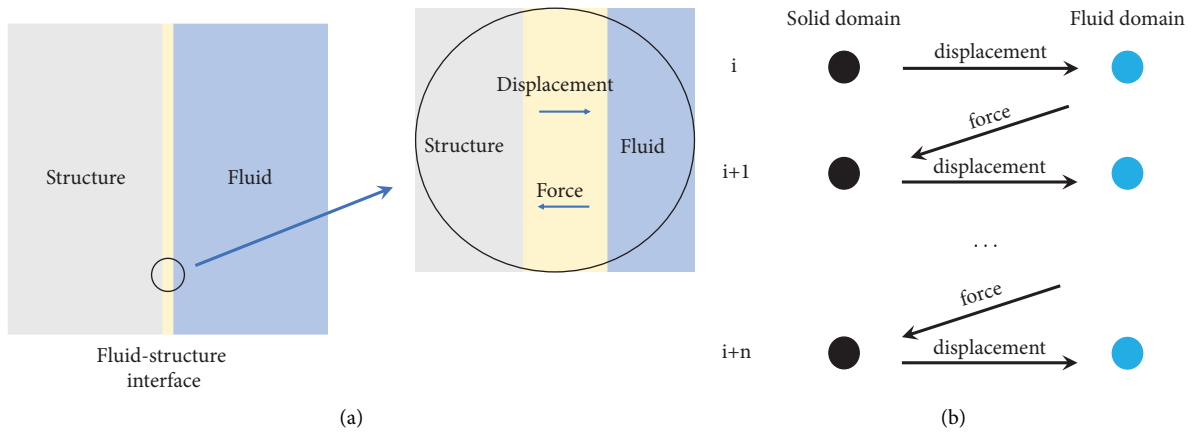

Figure 4: Schematic diagram of fluid-structure coupling. (a) Fluid-structure interface. (b) Iteration and transfer of loads.

point, the number of fluid-domain and solid-domain grids was 47360 and 5548. In addition, for the fluid-domain grid, the hexahedral gridding method was used and a boundary layer grid was placed near the walls to improve the accuracy of the calculation. For the solid domain, the conventional hexahedral gridding method was used. The grid division and local details are shown in Figure 8.

3.4. Two-Way Fluid-Structure Coupling Calculation Method Verification. For the fluid-domain section, the correction CFD-PBM model of gas-liquid two-phase flow was used for transient calculations with the calculation with convergence precision of 10^{-3}. In addition, the standard k-epsilon turbulence model was used in this paper, and the UDF program was applied to define the velocity at the inlet.

In addition, to verify the necessity of investigating the effect of bubbly fluids on the structural response, the structural response of the pipeline transporting a single-phase fluid was calculated with the aid of the two-way fluid-structure coupling calculation method and compared with the condition in the grid independence verification above. The acceleration amplitude at the outlet of the pipeline was chosen for comparison. The results are shown in Figure 9.

Figure 9 shows the distribution of acceleration amplitudes at the outlet of the pipeline driven by single-phase and two-phase flow. As shown in the figure, the overall distribution of the two curves had a similar trend, with a peak in acceleration amplitude around 3.7 seconds. However, there was a relatively large difference in the peak magnitude of the two curves. The extreme value of the amplitude is 26.05 mm when transporting single-phase flow. For the condition of two-phase flow, there was a significant increase in the limit of amplitude to 215.68 mm. It was apparent that the two-phase flow had an obvious effect on the structural response compared to the single-phase flow.

Furthermore, for the two-way fluid-structure coupling method used in this paper, the deformation of the structure was very small and the effect on the flow field distribution in the pipeline was almost negligible according to the literature [4]. The aim of this paper was to investigate the structural response of the pipe wall, so it was necessary to apply the two-way fluid-structure coupling method to solve the response of the pipe wall under the internal fluid drive.

4. Experimental Verification

To verify the accuracy of the numerical calculation method used in this paper, a pipeline made of PC material was used for the scaling experiment. The experimental scene is shown in Figure 10.

4.1. Models and Boundary Conditions. The scaling experiment conducted in this paper was carried out in the Marine Engineering Laboratory of Jiangsu University of Science and Technology. The scaling ratio of this model was 1 : 10, the material was PC, and the relevant material parameters are shown in Table 2. To correspond to the boundary conditions of the numerical simulation model, a metal clamp were used on the left side of the model to simulate the fixed end constraint boundary conditions. In addition, the ends of the supports were glued to the ground to simulate the fixed end constraint boundary conditions, as shown in Figure 7.

4.2. Experimental Design and Data Acquisition. The scaling experiment was designed to estimate the vibration response of the pipeline under different excitation conditions. In order to control the flow velocity in the pipeline, the ultrasonic flow sensor was placed in the middle of the pipeline to detect the velocity, and the measurement error of the instrument was ±1%. In addition, a triaxial piezoelectric vibration sensor was arranged at the outlet of the pipeline to collect the vibration signal, and the resolution ratio of the instrument was ±0.004 m/s^2. The sampling rate of the system was 100 Hz. To minimize the influence of the mass of the sensor on the vibration conditions at the outlet, the sensor with the lowest mass (12 g) to meet the measuring range requirement was chosen for the

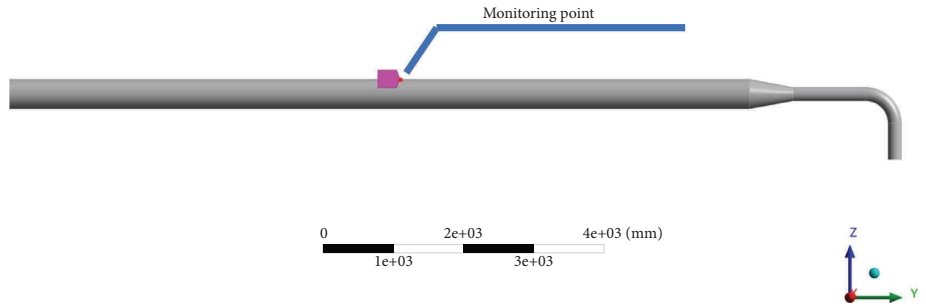

Figure 5: Diagram of the location of the monitoring point.

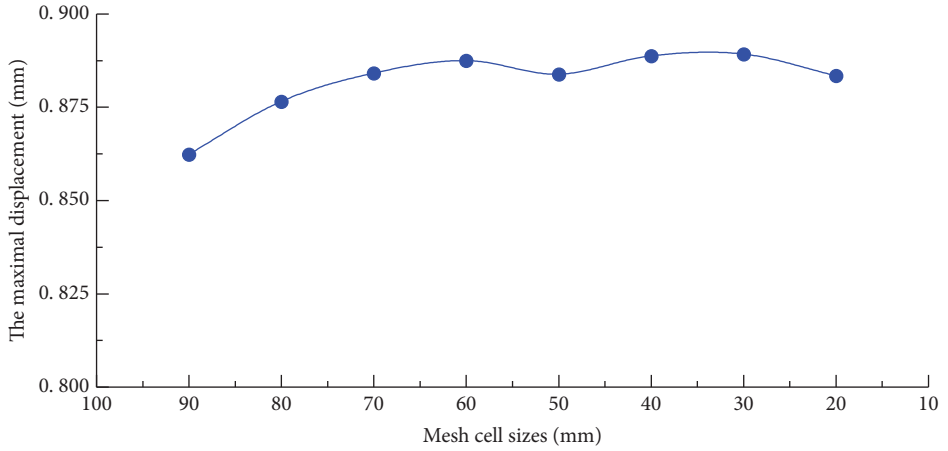

Figure 6: Diagram of grid-independent verification results.

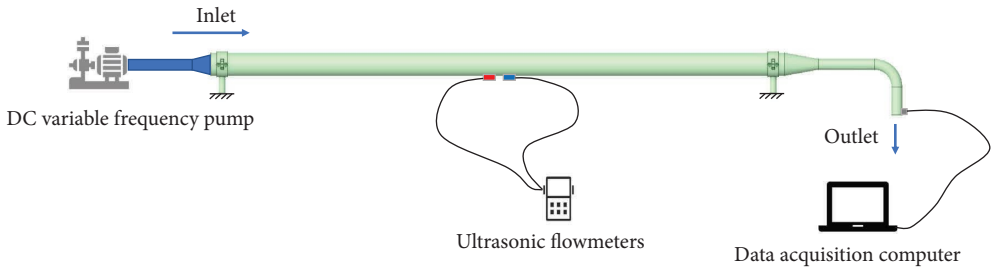

Figure 7: Diagram of the experimental principle.

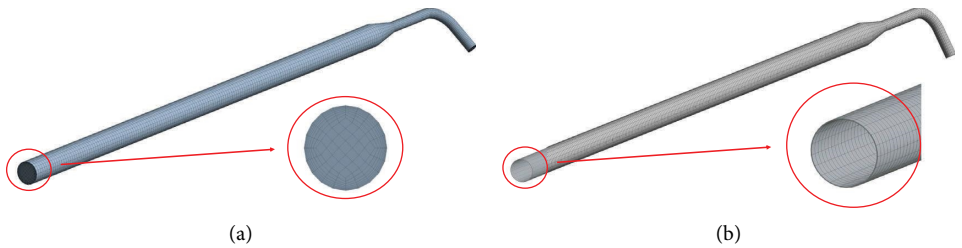

Figure 8: Schematic diagram of the grid division of pipeline structure. (a) Solid-domain meshes. (b) Fluid-domain meshes.

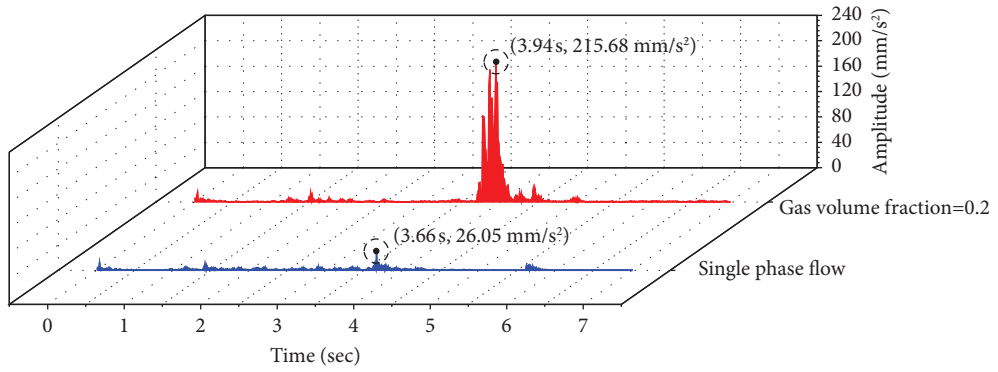

Figure 9: Diagram for comparison of structural response between single-phase flow and two-phase flow.

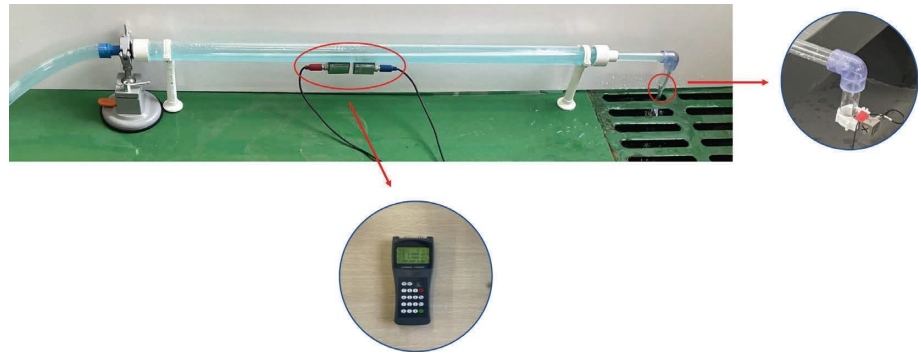

Figure 10: Diagram of the experimental scene.

experiment and was attached to the surface of the outlet using 3M adhesive. On the basis of meeting the relevant measurement requirements, the flow velocity at the inlet was adjusted using a DC variable frequency pump. The layout of the equipment is shown in Figure 10.

5. Calculation and Experimental Results and Analysis

5.1. Analysis of Results of the Scaling Experiment. Firstly, the flow field distribution of the pipeline was observed in this paper. The inlet velocities of the scaled and real scale models remained similar to the Froude number:

$$\begin{aligned} \mathrm{Fr} &= \frac{u_p}{\sqrt{gL_p}} \\ &= \frac{u_m}{\sqrt{gL_m}}, \end{aligned} \tag{16}$$

where u_p and u_m are the inlet velocities of the scaled and real scale models and L_p and L_m are the geometric dimensions of the scaled and real scale models.

As the scaling ratio of the model investigated in this paper was 1 : 10, when the inlet velocity of the real scale model was 2 m/s, we could get the inlet velocity of the scaled model to be 0.6 m/s with the help of equation (16). The distributions of the flow field derived from experimental observations as well as numerical calculations are shown in Figure 11.

Table 2: Material parameters of the scaling model.

Density (kg/m^3)	Poisson's ratio	Young's modulus (MPa)
1200	0.39	2320

Figures 11(a) and 11(b) show the distributions of the flow field in the pipeline without and with bubbles when the flow regime is stable. As shown in the figure, the shape and length of the cavitation segments shown in the scaling experiment were in general agreement with the results of the numerical simulation. For Figure 11(a), the flow field in the pipeline was relatively stable, with only small bubble section forming at the top of the straight near the outlet due to the backflow of air. For Figure 11(b), the flow field was more turbulent and the upper part of the straight section was occupied by dense bubbles which accumulated towards the inlet. Therefore, there was a large volume of the empty bubbly area near the inlet. It could be seen that when the high bubble-filled two-phase flow was transported in the pipeline, the flow pattern in the pipeline was considerably different compared to the normal situation.

Therefore, this paper proceeded to build a finite element model concerning the dimensions of the scaled model for numerical calculations and monitored the acceleration amplitude at the outlet and compared it with the experimental results. Again, the model was verified for grid independence before the formal calculations began. Two

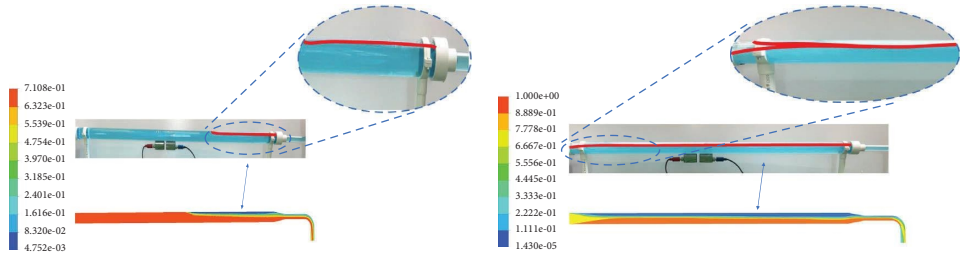

(a) (b)

Figure 11: Diagram of the distributions of the flow field. (a) Without bubbles. (b) With bubbles (gas volume fraction = 0.3).

operating conditions with inlet velocity = 0.4 and 0.6 m/s were selected for comparison. The sample intervals chosen are from the periods when the flow regime was stable. The relevant comparisons are shown below.

Figure 12(a) shows the comparison results between measured and simulated acceleration values when the inlet velocities are 0.4 and 0.6 m/s without bubbles. The left diagram shows the complete numerical simulation results. The period when the flow regime was stable was selected for comparison with the measured. To make a better comparison between the measured and simulated values, the frequency-domain analysis was performed on the selected data. For the condition with an inlet velocity of 0.4 m/s, when the frequency was 0.035 Hz, the acceleration amplitude of the simulated and measured value was 77.27 and 81.00 mm/s^2. Also, when the inlet velocity increased to 0.6 m/s, the acceleration amplitudes corresponding to this frequency (0.035 Hz) were 147.42 and 150.49 mm/s^2 for the measured and simulated values, respectively. The distribution of the two frequency curves showed that the simulated and measured values were in good agreement. Figure 12(b) shows the conditions with the addition of bubbles. Compared with the condition without bubbles, the main frequency increased to 0.055 Hz. Meanwhile, the acceleration amplitudes corresponding to this frequency (0.55 Hz) increased notably. When the inlet velocity was 0.4 m/s, acceleration values for the simulated and measured acceleration corresponding to the main frequency were 88.04 and 91.52 mm/s^2, respectively. As the inlet velocity increased to 0.6 m/s, these two values increased to 176.43 and 174.60 mm/s^2. In addition, the distribution of the two frequency curves showed that the simulated and measured values were also in good agreement.

5.2. Transient Analysis of Structural Response of Real Scale Pipelines. The previous section illustrated the reliability of the numerical calculation method used in this paper by means of numerical calculations and experimental verification based on the scaled model. It was also shown that the addition of bubbles had a significant effect on the vibration characteristics of the pipeline. Therefore, this section discussed the influence of the inlet velocity and inlet gas volume fraction on the vibration characteristics of the pipeline using a numerical simulation method based on the real scale model.

5.2.1. Comparison of Structural Response under Different Gas Volume Fractions. In the actual pipeline conveying process, the structural response characteristics of the pipeline vary greatly at different gas volume fractions. Therefore, this paper considered the actual load conditions and selected five conditions with gas volume fractions of 0.1, 0.2, 0.3, 0.4, and 0.5 for calculation. The velocity at the inlet was also defined using the UDF, with a velocity of 2 m/s at a steady state. In addition, the carbon dioxide was also in the form of bubbles with a diameter of 1.1 to 1.2 mm at the inlet.

After calculations, the overall vibration amplitude was higher in the middle of the straight pipe section and at the outlet due to the long distance from the support.

Figure 14 shows the location of the monitoring point. After determining the location of the monitoring point, the acceleration values at the point were chosen to characterize the strength of the vibration.

Figure 15shows the vibration response of monitoring points at different gas volume fractions over the calculation time. It could be seen from the figure that the trend in the vibration response of the monitoring points over time is broadly consistent. In the range of 0 to 0.1 s, there was a relatively large acceleration at the monitoring point at moment 0 due to the gradual application of the load inside the pipeline. In the range of 0.1 to 3.5 s, the medium in the pipeline flowed mainly through the straight area, so the monitoring points exhibited a relatively smooth vibration response condition. At the time around 3.5 s, the medium flowed through the bend area. The flow field distribution in the pipeline was gradually complicated, and the pressure distribution on the pipe wall was not uniform, causing the response of the structure to increase. However, as the gas volume fraction increased, the spots where the acceleration values increased sharply at the monitoring points gradually postponed, the maximum values gradually increased, and the time interval of structural instability became longer. Corresponding to the above typical moments, the flow field distribution in the pipeline was as follows.

Figure 13 shows the measured acceleration amplitude at the outlet with and without bubbles for two inlet velocities. As shown in the figure, with the addition of bubbles, the fluctuation range of the acceleration amplitude increased significantly and the mean vibration amplitudes had an increase of 19.7% and 17.9% compared to the former case.

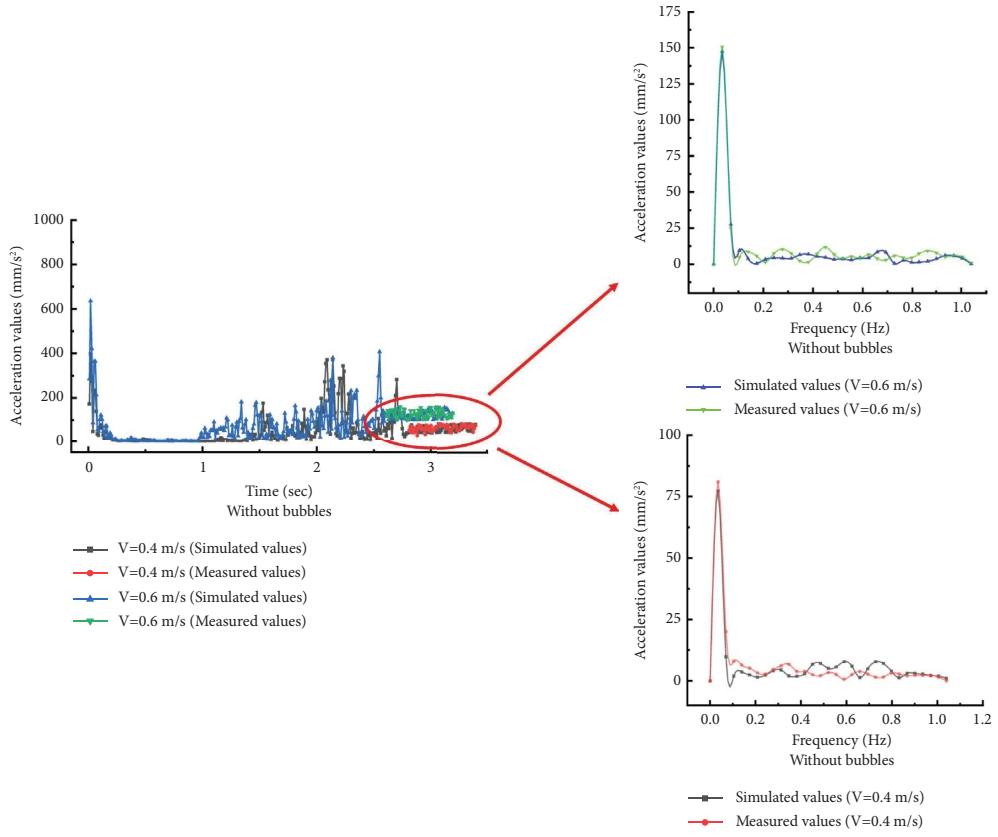

(a)

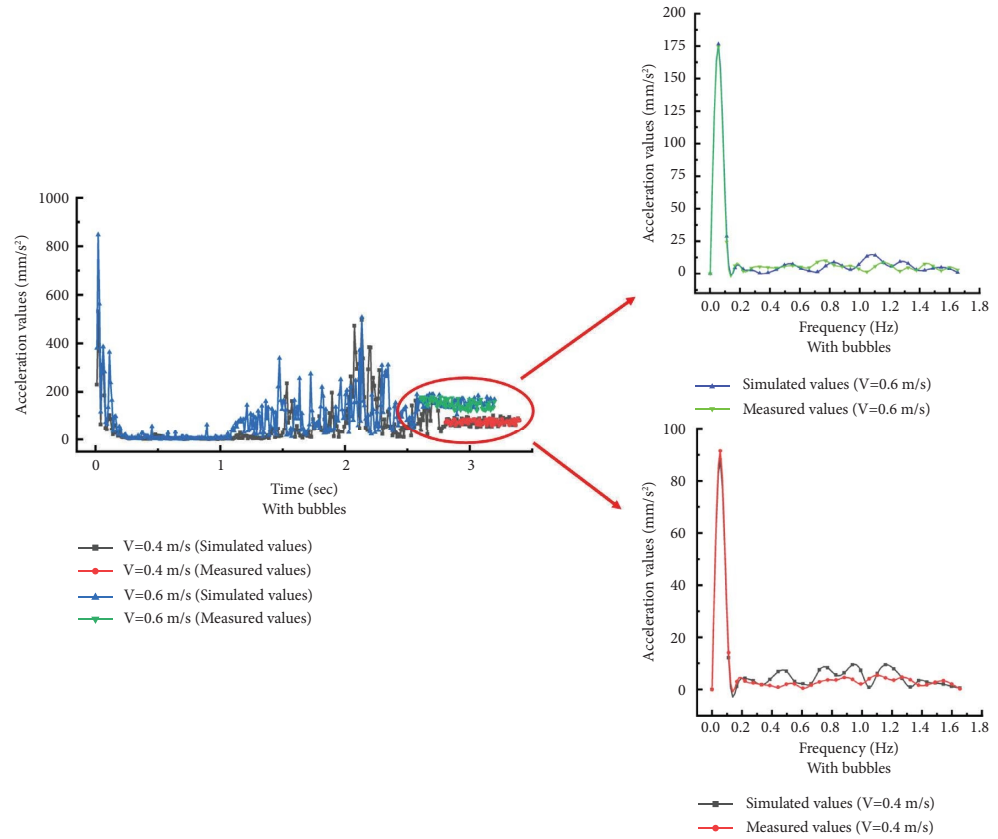

(b)

Figure 12: Diagram of the comparison results between measured and simulated acceleration values. (a) Without bubbles. (b) With bubbles.

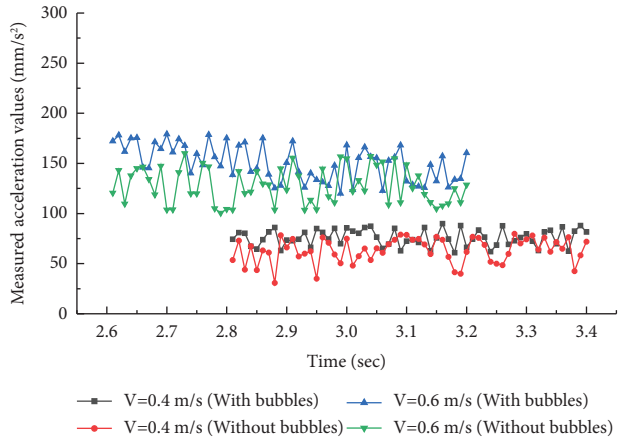

Figure 13: Diagram of the measured acceleration values.

This showed that the addition of bubbles had a significant effect on the vibration of the pipeline.

Figure 16 shows the distribution of the water volume fraction in the pipeline at several typical moments for three operating conditions with gas volume fractions of 0.1, 0.3, and 0.5. As the gas volume fraction increased, the time for the water to reach the bend section gradually lagged behind, while the period to flow through the bend area also gradually increased. To analyze this phenomenon, the accumulation of carbon dioxide bubbles in the upper part of the pipe wall had a certain blocking effect on the transport of liquid below, so it showed that as the gas volume fraction increased, the time for the liquid to reach the bend area gradually lagged behind. This local blocking phenomenon is consistent with the results in [37, 38]. Meanwhile, the bubbles were influenced by the shape of the pipeline in the reducer and bend area and accumulated towards the inlet, causing a reduction in the liquid volume fraction at the inlet, and the degree of reduction increased with the increase of gas volume fraction. When the liquid was transported to the bend area, the pressure decreased due to the closeness to the outlet, bubbles existed to precipitate and break, the flow field became unstable, and the acceleration response of the structure increased at the same time. The degree of instability increased to a certain extent as the gas volume fraction increased.

Next, the collected acceleration time data were processed using the fast Fourier transform method to transform the time-domain signal of the vibration response of monitoring point B into a frequency-domain signal, as shown in Figure 17.

Figure 17 shows the frequency-domain analysis results of the vibration response of monitoring point B at different gas volume fractions. As shown in the figure, according to the results of the frequency-domain analysis of the values at monitoring point B, the main frequency of the acceleration response at the outlet position was around 0.25 Hz for different gas volume fractions. The main frequency obtained there was closer to the value measured by the experiment investigated in [39]. The maximum acceleration values corresponding to the main frequency for different gas volume fraction conditions were discussed next.

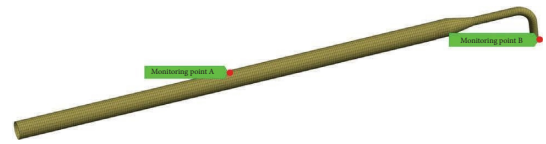

Figure 14: Diagram of the location of the monitoring point.

As shown in the figure, when the gas volume was 0.1 and 0.2, the maximum acceleration values for the main frequency were close to each other, both around 9.7 mm/s^2. When the gas volume fraction was increased to 0.3, there was a large increase in the maximum acceleration values, reaching 22.05 mm/s^2, with an increase of 126%, whereas the value was increased to 0.4, and the maximum acceleration value corresponding to the main frequency had another large increase of 30.97 mm/s^2. %. The increase in the maximum acceleration values corresponding to the main frequencybetween gas fractions0.3 and 0.4 decreased compared to the value between volume fractions 0.2 and 0.3, which was only 40.45%. Finally, when the gas volume fraction was increased to 0.5, the maximum acceleration value corresponding to the main frequency was close to those of 0.4, being 31.02 mm/s^2. Therefore, in the real ship scene, the surge in acceleration amplitude due to an increase in gas volume fraction was a priority.

5.2.2. Comparison of Structural Response under Different Inlet Velocities. In the actual pipeline conveying process, the structural response characteristics of the pipeline could also be influenced by the input velocity of the medium at the inlet. Therefore, this paper considered the actual load conditions and selected five conditions with an inlet velocity of 1, 2, 3, 4, and 5 m/s for calculation. The velocity was also defined using UDF and increased linearly to the corresponding steady-state value at 0.1 s. In addition, the carbon dioxide gas was also in the form of bubbles with a diameter of 1.1 to 1.2 mm and the gas volume fraction was chosen to take into account the large acceleration amplitude operating conditions in Section 5.2.1 and was finally determined to be 0.4.

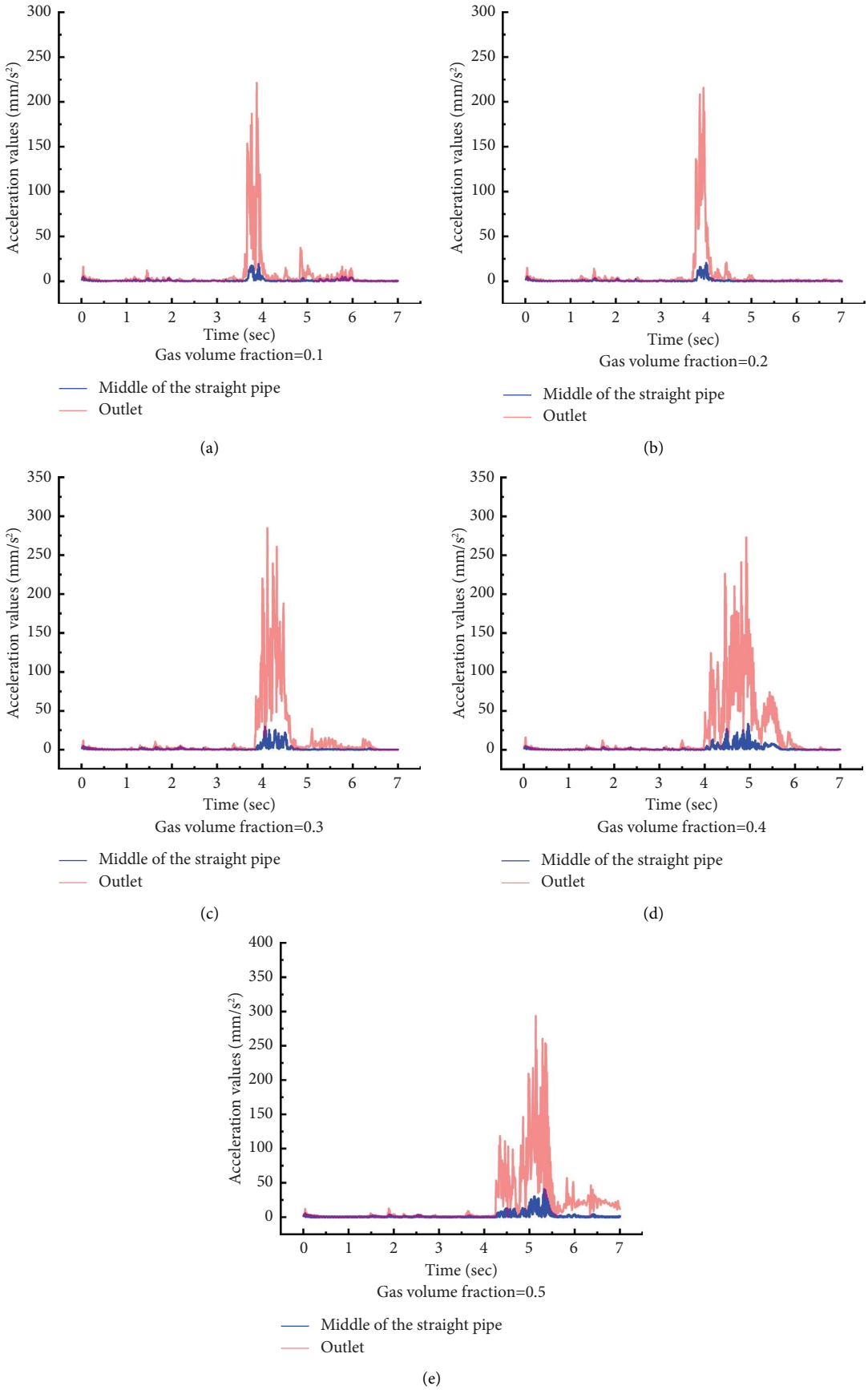

Figure 15: The time-domain diagram of the vibration response of monitoring points at different gas volume fractions. (a) Volume fraction = 0.1. (b) Volume fraction = 0.2. (c) Volume fraction = 0.3. (d) Volume fraction = 0.4. (e) Volume fraction = 0.5.

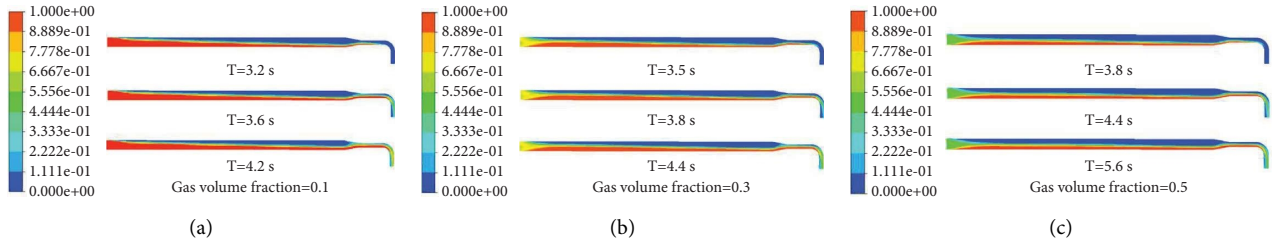

Figure 16: Diagram of the distribution of the water volume fraction in the pipeline at several typical moments. (a) Gas volume fraction = 0.1. (b) Gas volume fraction = 0.3. (c) Gas volume fraction = 0.5.

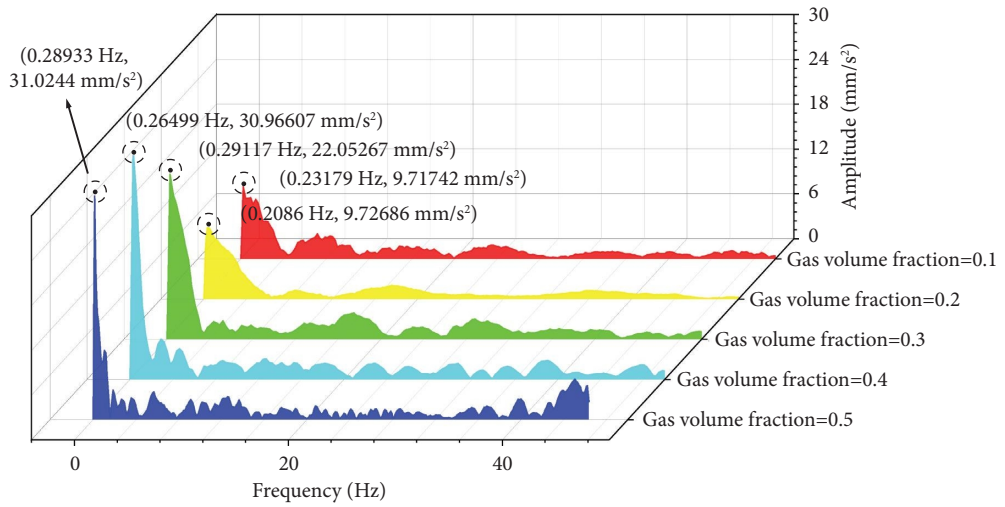

Figure 17: The frequency-domain diagram of the vibration response of monitoring point B at different gas volume fractions.

In this paper, relevant calculations were performed for the five operating conditions mentioned above, and the acceleration values at monitoring point B at the outlet were selected to signify the vibration of the pipeline.

Figure 18 shows the frequency-domain analysis results of the vibration response of monitoring point B at different inlet velocities, and Figure 18 shows the diagram of the maximum acceleration values corresponding to the main frequency for different inlet velocities. As shown in the figure, when the inlet velocity varied, the frequencies excited varied between 0.2 and 0.45 Hz, which were low-frequency vibrations.

Next, the maximum values of the acceleration obtained from the frequency-domain analysis were compared for different inlet velocities. As shown in the figure, when the inlet velocity was equal to or greater than 3 m/s, the calculated acceleration value gradually increased as the inlet velocity increased, a trend that was consistent with that described in [40]. However, when the inlet velocity was 1 and 2 m/s, the calculated acceleration values were much greater than those between 3 and 5 m/s. In particular, when the inlet velocity was 2 m/s, the acceleration value corresponding to the main frequency was 30.96607 mm/s^2, almost two and a half times the maximum acceleration value obtained from the operating conditions that the inlet velocities were between 3 and 5 m/s.

The following was an analysis of this phenomenon. The length of the flat section of the pipeline was about 10 m, and when the inlet velocity of the fluid medium was 2 m/s, the excitation frequency it induced was around 0.25 Hz. While the main frequency of the structure was concentrated between 0.2 and 0.45 Hz when the excitation frequency of the fluid medium was 0.25 Hz, a certain degree of structural resonance was generated, so a large acceleration value was shown in the figure. In practical operating conditions, the structural resonance phenomenon that existed when fluids were transferred at low speeds was more dangerous. Therefore, for the luxury passenger ship pipeline system studied in this paper, the problem of low-frequency resonance problem caused by the structural scale effect under the excitation of the fluid medium should be a key concern in its structural design process.

6. Structural Optimization of Pipeline Supports considering Vibrations

In the actual design of the ship pipeline system, the pipeline was often fixed by means of support restraint to avoid interference problems such as the collision between the pipeline and hull structure [41, 42]. In particular, for the luxury passenger ship life area pipeline system studied in this paper, the low-frequency vibration condition stated in the

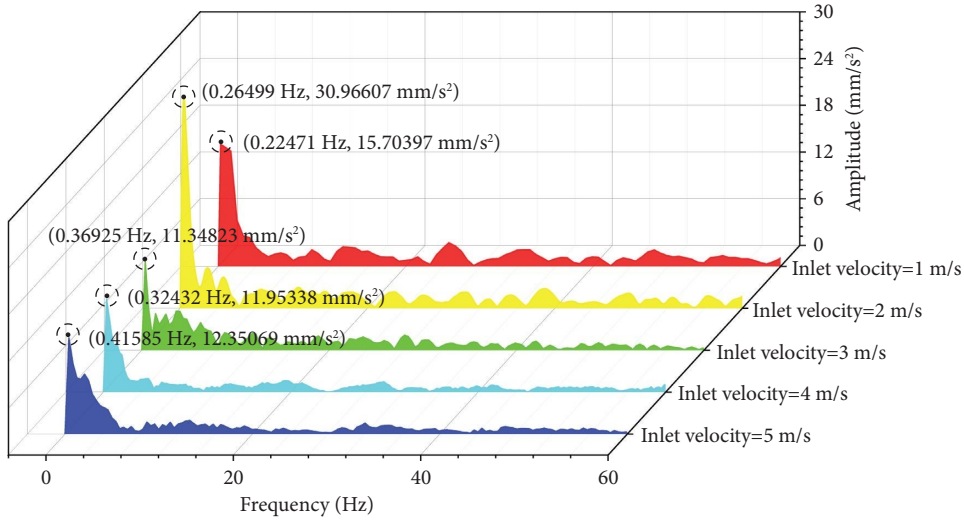

Figure 18: The frequency-domain diagram of the vibration response of monitoring point B at different inlet velocities.

section was to be strongly avoided due to the requirement for quietness. Therefore, this section compared the effects of different pipeline restraint forms on pipeline vibration based on the risky operating conditions calculated in Section 5.2.2 (inlet velocity = 2 m/s and gas volume fraction = 0.4) and provided a reference for the design of pipeline vibration control.

Two main measures were used in this section to reduce the vibration of the pipeline.

Option 1: adding support in the middle of the straight section to reduce the distance between supports and adding rubber washers to the contact area between the supports and the pipe wall.

Option 2: applying the rubber coating to the outer wall of the pipeline.

The structure of the two options is shown in Figure 19, and the parameters of the damping materials are shown in Table 3. The material properties here were presented using the Mooney–Rivlin hyperplastic model.

6.1. Comparison of the Vibration Reduction Effect of the Two Solutions. The comparison of the reduction effect of the two solutions was presented next. The degree of vibration was also assessed using acceleration data from monitoring B. Firstly, the acceleration values at monitoring point B were analyzed to derive the acceleration response in the time domain for the two optimization methods. Subsequently, the FFT method was performed on the acceleration values to obtain their distribution in the frequency domain. The relevant results are shown in Figure 20.

Figure 20 shows the relevant results of time-domain and frequency-domain analysis. Firstly, in the time domain, the maximum acceleration value of the structure in the initial state was 272.8 mm/s^2. When the structure was modified, the acceleration values of the pipeline were substantially reduced. At this time, the maximum acceleration values for options 1 and 2 were 10.165 and 176.44 mm/s^2. Comparing the maximum acceleration values at monitoring point B for the two options, option 1 provided better control of the extreme values. Furthermore, in terms of the time-domain curve, option 2 reduced the values of the maximum acceleration compared with the initial state, but there was an intensive alternation of accelerations over the period of 4 to 6 s. In contrast, option 2 provided a more stable control of the vibration acceleration.

Next, in the frequency domain, the main frequency of the structure in the initial state was 0.26499 Hz, corresponding to an acceleration value of 30.96607 mm/s^2. With option 2, the main frequency of the structure increased slightly to 0.304469 Hz. At this point, the acceleration value corresponding to the main frequency was 15.94452 mm/s^2, showing a considerable reduction compared to the initial state. However, the frequency-domain curve for option 2 had a small peak near 60 Hz, where the acceleration value was 3.93318 mm/s^2. When the external excitation frequency was close to this range, the structure was at risk of increased acceleration values. However, the frequency-domain curve for option 1 was relatively smooth overall, with a maximum acceleration value of 0.66397 mm/s^2, when the main frequency was 0.67036 Hz [43]. The trend of the effect of the support on the acceleration amplitude signal at the measurement point was consistent with the results in [44, 45]. This was a side indication of the reliability of the results of this experiment.

Finally, in terms of the feasibility of installing the pipeline, the method of laying a damping coating on the surface of the pipe was limited by the shape of the pipe wall, making the overall production more difficult and less economical. However, the method of reducing the distance between the supports and equipping rubber washers between the pipe wall and the supports was less difficult and more economical to install.

Therefore, taking into account the damping performance and the feasibility of installation, option 1 was the better choice.

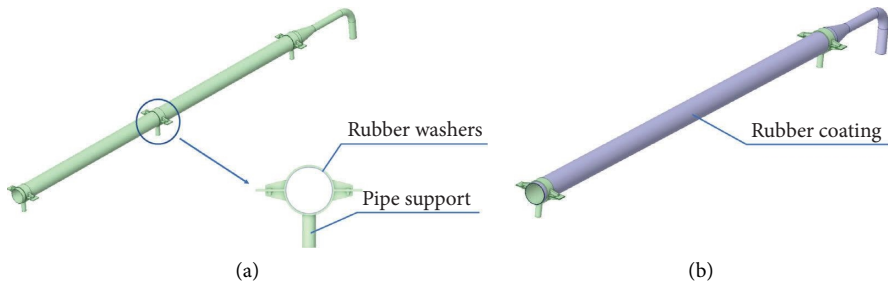

Figure 19: Diagram of the optimization of the pipeline structure. (a) Option 1. (b) Option 2.

Table 3: Parameters of the damping material.

Density (kg/m^3)	C10 (MPa)	C01 (MPa)	D1 (MPa^{-1})
1200	50	10	0.1

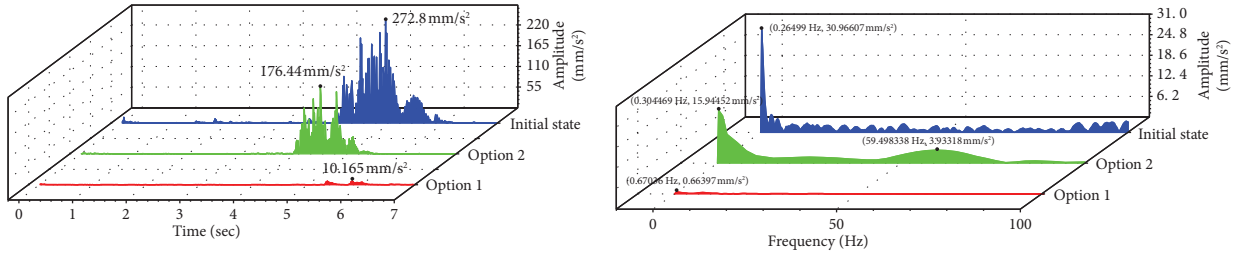

Figure 20: Time-domain and frequency-domain analysis results of the acceleration values at monitoring point B under different optimization methods. (a) Time domain. (b) Frequency domain.

6.2. Scaling Experiment Verification of Optimization Scheme. In order to verify the validity of option 1 as described in Section 6, this section validated it with the aid of the scaling experiment. The trial site and equipment conditions remained the same as described above, and the experimental scene is shown in Figure 21.

As shown in the figure, a support was added to the middle of the straight pipeline to reduce the distance between them. Conditions with inlet velocities of 0.3, 0.4, 0.5, and 0.6 m/s were selected, and the acceleration values at the monitoring points under different numbers of supports were collected and compared. Mean and standard deviation analyses were performed on the collected data, and the results of the correlation analysis are shown in Figure 22 and Table 4.

Figure 22 shows the acceleration amplitude at the outlet before and after optimization. As shown in the figure, the overall trend of the fitted plots obtained from the collected data points all fluctuated within the interval around the mean value. The addition of a central support could effectively reduce the mean value of the vibration, while the magnitude of the oscillations was also significantly reduced. As shown in Table 4, with the increase in inlet velocity, the mean acceleration values increased both before and after the addition of the central support, but the difference between the two sets of values increased. When the inlet velocity was 0.3 m/s, the difference was 11.70137 mm/s^2. But when the inlet velocity increased to 0.6 m/s, the difference increased considerably to 52.979 mm/s^2. It could be seen that the addition of the central support could effectively reduce the mean acceleration values of vibration, and its damping amplitude increased with the increase of inlet velocity. Next, the standard deviations of the values were analyzed. With the addition of the central support, the standard deviation acceleration values of vibration decreased considerably, and the difference between the two sets of values also increased with the increase of inlet velocity. This showed that with the addition of the central support, the distribution of acceleration values was more regular and amplitude was smaller compared with the initial condition, which was beneficial in reducing damage to the pipeline structure [44, 45].

In summary, optimizing the distance between supports could effectively reduce the mean values and

Figure 21: Diagram of the experimental scene.

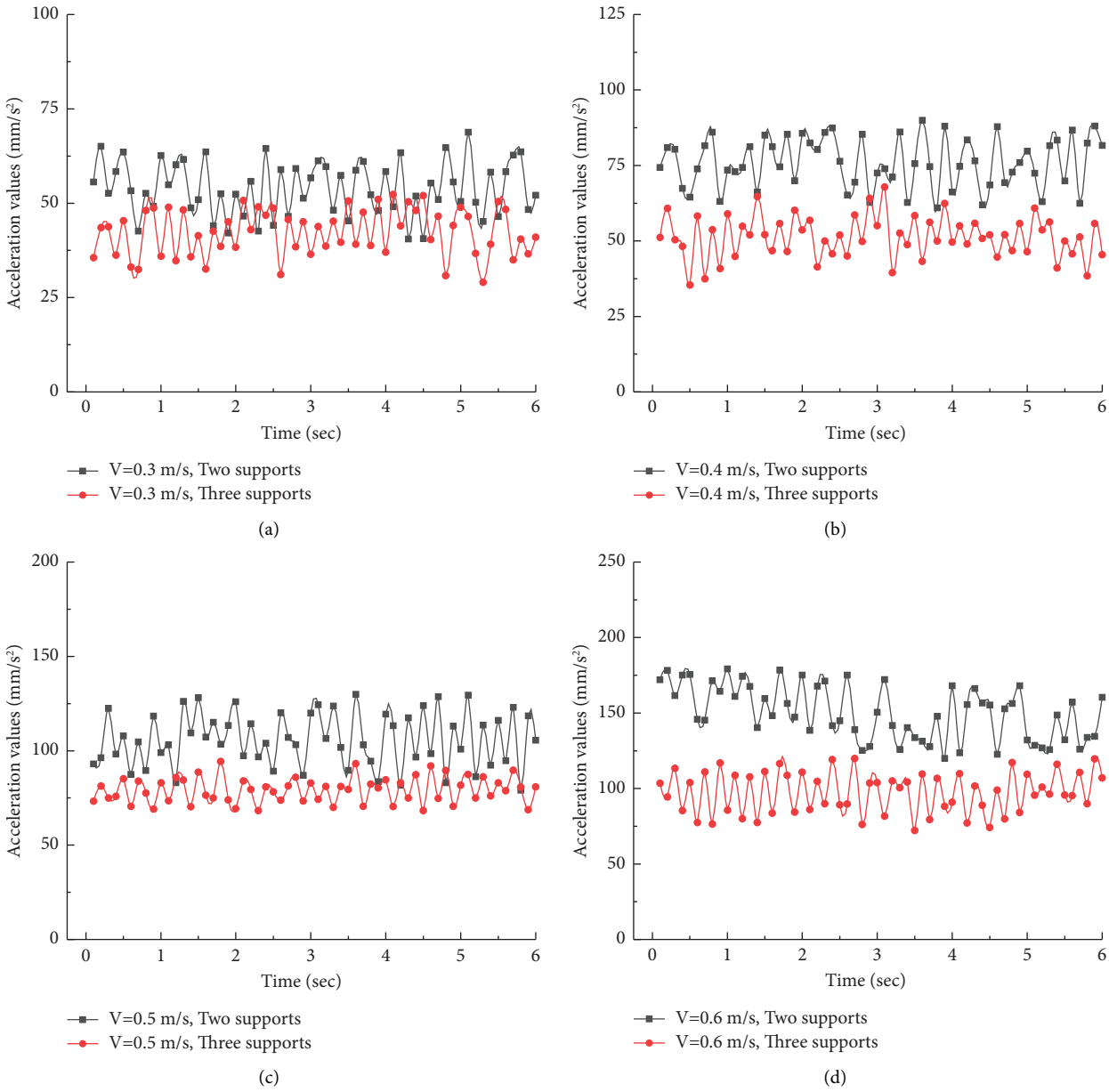

Figure 22: Diagram of the acceleration amplitude before and after optimization. (a) $V = 0.3$ m/s. (b) $V = 0.4$ m/s. (c) $V = 0.5$ m/s. (d) $V = 0.6$ m/s.

Table 4: Mean and standard deviation values.

	Two supports				Three supports			
Inlet velocity (m/s)	0.3	0.4	0.5	0.6	0.3	0.4	0.5	0.6
Mean value (mm/s^2)	54.0057	76.0282	106.0608	150.5234	42.30433	51.3917	75.2512	97.5444
Standard deviation values (mm/s^2)	7.0978	8.2173	14.1149	17.7938	6.1346	6.9508	7.7334	13.6241

fluctuation of pipeline vibration. In addition, the combination of rubber washers could be used to get better vibration damping.

7. Conclusions

This paper mainly investigated the vibration characteristics of pipelines transporting bubbly fluid medium, and a typical pipeline structure in a luxury passenger ship life area was selected as the object of study. A two-way fluid-structure coupling analysis was carried out with the aid of ANSYS software, and the PBM model was introduced to characterize the dynamic properties of bubbles. On this basis, the response of the pipeline under different situations was calculated.

The main findings of this study could be summarized as follows:

(1) For the pipeline studied in this paper, when the inlet velocity and gas volume fraction were the same, the addition of bubbles had a great influence on the flow field distribution in the pipeline. The addition of bubbles made the high gas volume space in the upper part of the pipeline to grow significantly and extend to the inlet area. Meanwhile, the fluid medium was filled with dense bubbles and the instability of the flow field increased and vibration acceleration values increased significantly compared to the condition without the addition of bubbles.

(2) The inlet gas volume fraction and velocity had a great effect on the vibration characteristics of the pipeline. For the pipeline structure investigated in this paper, a sharp increase in vibration values occurred as the inlet gas volume fraction increased. In addition, for individual inlet conditions, the excitation and the inherent frequency of the structure were close and the structure appeared to resonate. The occurrence of this sharp increase in structural vibrations or even resonance related to the gradual change in the inlet condition should be given particular attention.

(3) Taking into account the damping performance and the feasibility of installation, the optimization method of reducing the distance between the supports and equipping rubber washers between the pipe wall and the supports provided excellent performance in terms of both economy and damping performance. The scaling experiment also demonstrated the feasibility of this method. This structural design idea could be used as a reference for the vibration damping design in the real pipeline system.

Data Availability

The data used to support the findings of the study are available from the corresponding author upon request.

Conflicts of Interest

The authors declare that they have no conflicts of interest.

Acknowledgments

The authors would like to acknowledge the financial support provided by Postgraduate Research & Practice Innovation Program of Jiangsu Province (KYCX_3838).

References

[1] G. Liu, S. Li, Y. Li, and H. Chen, "Vibration analysis of pipelines with arbitrary branches by absorbing transfer matrix method," *Journal of Sound and Vibration*, vol. 332, no. 24, pp. 6519–6536, 2013.

[2] S. J. Li, G. M. Liu, and W. T. Kong, "Vibration analysis of pipes conveying fluid by transfer matrix method," *Nuclear Engineering and Design*, vol. 266, pp. 78–88, 2014.

[3] S. Li, *Fluid-structure Coupling Dynamics Calculation and Characteristic Analysis of Pipeline System*Harbin Engineering University, Harbin, China, 2015.

[4] G. Wu, X. Zhao, D. Shi, and X. Wu, "Analysis of fluid-structure coupling vibration mechanism for subsea tree pipeline combined with fluent and ansys workbench," *Water*, vol. 13, no. 7, p. 955, 2021.

[5] Y. Zhen, Y. Gong, and Y. Tang, "Nonlinear vibration analysis of a supercritical fluid-conveying pipe made of functionally graded material with initial curvature," *Composite Structures*, vol. 268, Article ID 113980, 2021.

[6] M. Karpenko and M. Bogdevičius, "Investigation into the hydrodynamic processes of fitting connections for determining pressure losses of transport hydraulic drive," *Transport*, vol. 35, no. 1, pp. 108–120, 2020.

[7] T. Young, "Hydraulic investigations, subservient to an intended Croonian Lecture on the motion of the blood," *Philosophical Magazine*, vol. 33, no. 130, pp. 123–133, 1809.

[8] L. Cao, *Characteristic Analysis of Fluid-Structure Interaction*Kunming University of Science and Technology, Kunming, China, 2004.

[9] N. Joukowsky, "On the hydraulic hammer in water supply pipes," in *Proceedings of the American Water Works Association*, pp. 341–424, Toronto, Canada, June 1904.

[10] D. C. Wiggert, F. J. Hatfield, and S. Stuckenbruck, "Analysis of liquid and structural transients in piping by the method of characteristics," *Journal of Fluids Engineering*, vol. 109, no. 2, pp. 161–165, 1987.

[11] D. C. Wiggert and A. S. Tijsseling, "Fluid transients and fluid-structure interaction in flexible liquid-filled piping," *Applied Mechanics Reviews*, vol. 54, no. 5, pp. 455–481, 2001.

[12] A. F. D'Souza and R. Oldenburger, "Dynamic response of fluid lines," *Journal of Basic Engineering*, vol. 86, no. 3, pp. 589–598, 1964.

[13] A. R. D. Thorley, "Pressure transients in hydraulic pipelines," *Journal of Basic Engineering*, vol. 91, no. 3, pp. 453–460, 1969.

[14] F. T. Brown, "The transient response of fluid lines," *Journal of Basic Engineering*, vol. 84, no. 4, pp. 547–553, 1962.

[15] F. T. Brown, "A quasi method of characteristics with application to fluid lines with frequency dependent wall shear and heat transfer," *Journal of Basic Engineering*, vol. 91, no. 2, pp. 217–226, 1969.

[16] E. L. Holmboe and W. T. Rouleau, "The effect of viscous shear on transients in liquid lines," *Journal of Basic Engineering*, vol. 89, no. 1, pp. 174–180, 1967.

[17] M. El-Raheb, "Vibrations of three-dimensional pipe systems with acoustic coupling," *Journal of Sound and Vibration*, vol. 78, no. 1, pp. 39–67, 1981.

[18] A. Ahmadi and A. R. Keramat, "Investigation of the junction coupling due to various types of the discrete points in a piping system," in *Proceedings of the 12th International Conference on Computer Methods and Advances in Geomechanics*, pp. 4016–4024, Goa, India, October 2008.

[19] M. Kubrak, A. Malesińska, A. Kodura, K. Urbanowicz, and M. Stosiak, "Hydraulic transients in viscoelastic pipeline system with sudden cross-section changes," *Energies*, vol. 14, no. 14, p. 4071, 2021.

[20] D. C. Wiggert, R. S. Otwell, and F. Hatfield, "The effect of elbow restraint on pressure transients journal of fluids engineering," *Journal of Fluids Engineering*, vol. 107, no. 3, 1985.

[21] J. F. Whatham, "Analysis of pipe bends with symmetrical noncircular cross sections," *Journal of Applied Mechanics*, vol. 54, no. 3, pp. 604–610, 1987.

[22] R. A. Clark, T. I. Gilroy, and E. Reissner, "Stresses and deformations of toroidal shells of elliptical cross section: with applications to the problems of bending of curved tubes and of the Bourdon gage," *Journal of Applied Mechanics*, vol. 19, no. 1, pp. 37–48, 2021.

[23] J. S. Walker and J. W. Phillips, "Pulse propagation in fluid-filled tubes," *Journal of Applied Mechanics*, vol. 44, no. 1, pp. 31–35, 1977.

[24] F. J. Hatfield, D. C. Wiggert, and R. S. Otwell, "Fluid structure interaction in piping by component synthesis," *Journal of Fluids Engineering*, vol. 104, no. 3, pp. 318–325, 1982.

[25] S. C. Tentarelli, *Propagation of Noise and Vibration in Complex Hydraulic Tubing Systems*Lehigh University, Bethlehem, PA, USA, 1990.

[26] Y. Cheng, H. Oertel, and T. Schenkel, "Fluid-structure coupled CFD simulation of the left ventricular flow during filling phase," *Annals of Biomedical Engineering*, vol. 33, no. 5, pp. 567–576, 2005.

[27] M. Kuntz, J. C. Ferreira, F. R. Menter, and G. N. M. Oudendijk, "Analysis of fluid-structure interaction with an improved coupling strategy," in *Proceedings of the 3rd International Conference on Engineering Computational Technology*, pp. 85-86, Civil-Comp press, Prague, Czech Republic, September 2002.

[28] W. Qu, H. Zhang, W. Li, W. Sun, L. Zhao, and H. Ning, "Influence of support stiffness on dynamic characteristics of the hydraulic pipe subjected to basic vibration," *Shock and Vibration*, vol. 2018, Article ID 4035725, 8 pages, 2018.

[29] S. W. Liu Yong, "Study on pressure loss of liquid-solid two-phase flow in the pipeline under transverse bending vibration," *China Journal of Hydrodynamics*, vol. 34, no. 1, pp. 115–121, 2019.

[30] X. Z. Chen, Z. H. Luo, W. C. Yan, Y. H. Lu, and I. S. Ng, "Three-dimensional CFD-PBM coupled model of the temperature fields in fluidized-bed polymerization reactors," *AIChE Journal*, vol. 57, no. 12, pp. 3351–3366, 2011.

[31] B. Zhang, L. Kong, H. Jin, G. He, S. Yang, and X. Guo, "CFD simulation of gas–liquid flow in a high-pressure bubble column with a modified population balance model," *Chinese Journal of Chemical Engineering*, vol. 26, no. 6, pp. 1350–1358, 2018.

[32] F. Zhang, L. Zhu, K. Chen, W. Yan, D. Appiah, and B. Hu, "Numerical simulation of gas–liquid two-phase flow characteristics of centrifugal pump based on the CFD–PBM," *Mathematics*, vol. 8, no. 5, p. 769, 2020.

[33] S. Yan, S. Sun, X. Luo, S. Chen, C. Li, and J. Feng, "Numerical investigation on bubble distribution of a multistage centrifugal pump based on a population balance model," *Energies*, vol. 13, no. 4, p. 908, 2020.

[34] U. Manual, *Ansys Fluent 12.0*, Ansys, Canonsburg, PA, USA, 2009.

[35] M. J. Hounslow, R. L. Ryall, and V. R. Marshall, "A discretized population balance for nucleation, growth, and aggregation," *AIChE Journal*, vol. 34, no. 11, pp. 1821–1832, 1988.

[36] H. Luo and H. F. Svendsen, "Theoretical model for drop and bubble breakup in turbulent dispersions," *AIChE Journal*, vol. 42, no. 5, pp. 1225–1233, 1996.

[37] Y. Zhang, H.-F. Duan, and A. Keramat, "CFD-aided study on transient wave-blockage interaction in a pressurized fluid pipeline," *Engineering Applications of Computational Fluid Mechanics*, vol. 16, no. 1, pp. 1957–1973, 2022.

[38] R. Zanganeh, E. Jabbari, A. Tijsseling, and A. Keramat, "Fluid-structure interaction in transient-based extended defect detection of pipe walls," *Journal of Hydraulic Engineering*, vol. 146, no. 4, Article ID 04020015, 2020.

[39] X. X. Ma, *Investigation on the Characteristics of Flow and its Induced Vibration for Gas-Liquid Two-phase Flow in a U-Tube*Shandong University, Shandong, China, 2018.

[40] S. Li, *Research on Fluid Structure Interaction Characteristics of the Variable Diameter Pipe under Vibration Condition*Northeast Petroleum University, Daqing, China, 2014.

[41] D.-M. Lee, S.-Y. Kim, B.-Y. Moon, and G. J. Kang, "Layout design optimization of pipe system in ship engine room for space efficiency," *Journal of the Korean Society of Marine Engineering*, vol. 37, no. 7, pp. 784–791, 2013.

[42] H.-S. Han and W.-B. Jeong, "Parametric study of the vibration transmissibility for the rubber mount of the seawater-conveying pipe in a ship," *Journal of the Society of Naval Architects of Korea*, vol. 46, no. 3, pp. 290–302, 2009.

[43] H. K. Aliabadi, A. Ahmadi, and A. Keramat, "Frequency response of water hammer with fluid-structure interaction in a viscoelastic pipe," *Mechanical Systems and Signal Processing*, vol. 144, Article ID 106848, 2020.

[44] A. Keramat, M. Fathi-Moghadam, R. Zanganeh, M. Rahmanshahi, A. S. Tijsseling, and E. Jabbari, "Experimental investigation of transients-induced fluid–structure interaction in a pipeline with multiple-axial supports," *Journal of Fluids and Structures*, vol. 93, Article ID 102848, 2020.

[45] R. Zanganeh, A. Ahmadi, and A. Keramat, "Fluid–structure interaction with viscoelastic supports during water hammer in a pipeline," *Journal of Fluids and Structures*, vol. 54, pp. 215–234, 2015.